Langmuir Article

pubs.acs.org/Langmuir

Deposition of Coatings from Live Yeast Cells and Large Particles by "Convective-Sedimentation" Assembly

Lindsey B. Jerrim and Orlin D. Velev*

Department of Chemical and Biomolecular Engineering, North Carolina State University, Raleigh, North Carolina 27695

Received May 15, 2008. Revised Manuscript Received March 15, 2009

Convective assembly at high volume fraction was used for the rapid deposition of uniform, close-packed coatings of *Saccharomyces cerevisiae* yeast cells onto glass slides. A computational model was developed to calculate the thickness profiles of such coatings for different set of conditions. Both the experiments and the numerical simulations demonstrated that the deposition process is strongly affected by the presence of sedimentation. The deposition device was inclined to increase the uniformity of the coatings by causing the cells to sediment toward the three-phase contact line. In accordance with the simulation, the experiments showed that both increasing the angle of the device and decreasing the angle between the slides increased the uniformity of the deposited coatings. Finally, the "convective-sedimentation" assembly method was used to deposit mixed layers of live cells and large latex particles as an example of immobilized biologically active composite coatings.

Introduction

Close-packed and uniform films and coatings composed of colloidal particles have a wide variety of potential applications. One facile and simple process to organize and deposit the particles in a liquid film into crystalline and close-packed structures is convective assembly from drying menisci.[1,2] A wide variety of particle types have been deposited by this method, including colloidal latex,[1−6] gold nanoparticles,[7,8] anisometric zeolites,[9] and colloidal silica.[10,11] Many different applications for such coatings are being developed, including antireflective coatings,[10] surface-enhanced Raman spectroscopy (SERS) enhancement substrates for sensors,[8,12] materials for surface-assisted desorption/ionization mass spectrometry,[13] biosensors,[14] catalysis,[15] macroporous films,[8,16,17] and photonic crystals.[18−20]

Live eukaryotic microbial and animal cells present an interesting object for colloidal assembly as "particles of a kind."[21] A large number of cell deposition techniques have been investigated in recent years, and the resulting cell films represent interesting biomaterials. Most of the cell deposition techniques reported involve patterning, electrodes, or templating. Such methods include the use of electroactive substrates,[22] dielectrophoresis between microelectrodes,[21] modulated magnetic fields,[23] inkjet and laser printing,[24,25] optical trapping,[26] biologically friendly lithography,[27−29] covalent bonding to alkanethiols,[30] encapsulation with a polyelectrolyte,[31] laminar flow patterning[32] and droplet templating.[33] Several methods use polydimethylsiloxane

*Corresponding author. E-mail: odvelev@unity.ncsu.edu.

(1) Denkov, N. D.; Velev, O. D.; Kralchevsky, P. A.; Ivanov, I. B.; Yoshimura, H.; Nagayama, K. *Langmuir* **1992**, *8*, 3183–3190.
(2) Denkov, N. D.; Velev, O. D.; Kralchevsky, P. A.; Ivanov, I. B.; Yoshimura, H.; Nagayama, K. *Nature (London)* **1993**, *361*, 26.
(3) Dimitrov, A. S.; Nagayama, K. *Chem. Phys. Lett*. **1995**, *243*, 462–468.
(4) Dimitrov, A. S.; Nagayama, K. *Langmuir* **1996**, *12*, 1303–1311.
(5) Dushkin, C. D.; Yoshimura, H.; Nagayama, K. *Chem. Phys. Lett*. **1993**, *204*, 455–460.
(6) Prevo, B. G.; Velev, O. D. *Langmuir* **2004**, *20*, 2099–2107.
(7) Prevo, B. G.; Fuller, J. C.; Velev, O. D. *Chem. Mater*. **2005**, *17* 28–35.
(8) Kuncicky, D. M.; Christesen, S. D.; Velev, O. D. *Appl. Spectrosc*. **2005**, *59*, 401–409.
(9) Lee, J. A.; Meng, L. L.; Norris, D. J.; Scriven, L. E.; Tsapatsis, M. *Langmuir* **2006**, *22*, 5217–5219.
(10) Prevo, B. G.; Hwang, Y.; Velev, O. D. *Chem. Mater*. **2005**, *17* 3642–3651.
(11) Jiang, P.; Bertone, J. F.; Hwang, K. S.; Colvin, V. L. *Chem. Mater*. **1999**, *11*, 2132–2140.
(12) Freeman, R. G.; Grabar, K. C.; Allison, K. J.; Bright, R. M.; Davis, J. A.; Guthrie, A. P.; Hommer, M. B.; Jackson, M. A.; Smith, P. C.; Walter, D. G.; Natan, M. J. *Science* **1995**, *267*, 1629–1632.
(13) Finkel, N. H.; Prevo, B. G.; Velev, O. D.; He, L. *Anal. Chem*. **2005**, *77*, 1088–1095.
(14) Wang, K.; Xu, J. J.; Chen, H. Y. *Sens. Actuators, B: Chem*. **2006**, *114*, 1052–1058.
(15) Yagi, M.; Tomita, E.; Sakita, S.; Kuwabara, T.; Nagai, K. *J. Phys. Chem. B* **2005**, *109*, 21489–21491.
(16) Turner, M. E.; Trentler, T. J.; Colvin, V. L. *Adv. Mater*. **2001**, *13* 180–183.
(17) Jiang, P.; Cizeron, J.; Bertone, J. F.; Colvin, V. L. *J. Am. Chem. Soc*. **1999**, *121*, 7957–7958.
(18) Kalkman, J.; de Bres, E.; Polman, A.; Jun, Y.; Norris, D. J.; 't Hart, D. C.; Hoogenboom, J. P.; van Blaaderen, A. *J. Appl. Phys*. **2004**, *95*, 2297–2302.
(19) Norris, D. J.; Vlasov, Y. A. *Adv. Mater*. **2001**, *13*, 371–376.
(20) Subramania, G.; Constant, K.; Biswas, R.; Sigalas, M. M.; Ho, K. M. *Appl. Phys. Lett*. **1999**, *74*, 3933–3935.
(21) Gupta, S.; Alargova, R. G.; Kilpatrick, P. K.; Velev, O. D. *Soft Matter* **2008**, *4*, 726–730.
(22) Yousaf, M. N.; Houseman, B. T.; Mrksich, M. *Proc. Natl. Acad. Sci. U.S. A*. **2001**, *98*, 5992–5996.
(23) Kimura, T.; Sato, Y.; Kimura, F.; Iwasaka, M.; Ueno, S. *Langmuir* **2005**, *21*, 830–832.
(24) Barron, J. A.; Spargo, B. J.; Ringeisen, B. R. *Appl. Phys. A: Mater. Sci. Process*. **2004**, *79*, 1027–1030.
(25) Roth, E. A.; Xu, T.; Das, M.; Gregory, C.; Hickman, J. J.; Boland, T. *Biomaterials* **2004**, *25*, 3707–3715.
(26) Odde, D. J.; Renn, M. *J. Biotechnol. Bioeng*. **2000**, *67*, 312–318.
(27) Karp, J. M.; Yeo, Y.; Geng, W.; Cannizarro, C.; Yan, K.; Kohane, D. S.; Vunjak-Novakovic, G.; Langer, R. S.; Radisic, M. *Biomaterials* **2006**, *27*, 4755–4764.
(28) Irimia, D.; Karlsson, J. O. M. *Biomed. Microdevices* **2003**, *5*, 185–194.
(29) Suh, K. Y.; Seong, J.; Khademhosseini, A.; Laibinis, P. E.; Langer, R. *Biomaterials* **2004**, *25*, 557–563.
(30) Veiseh, M.; Wickes, B. T.; Castner, D. G.; Zhang, M. *Biomaterials* **2004**, *25*, 3315–3324.
(31) Krol, S.; Nolte, M.; Diaspro, A.; Mazza, D.; Magrassi, R.; Gliozzi, A.; Fery, A. *Langmuir* **2005**, *21*, 705–709.
(32) Takayama, S.; McDonald, J. C.; Ostuni, E.; Liang, M. N.; Kenis, P. J. A.; Ismagilov, R. F.; Whitesides, G. M. *Proc. Natl. Acad. Sci. U.S.A*. **1999**, *96*, 5545–5548.
(33) Nellimoottil, T. T.; Rao, P. N.; Ghosh, S. S.; Chattopadhyay, A. *Langmuir* **2007**, *23*, 8655–8658.

(PDMS) to pattern substrates for cell growth.[34−37] Recently, it has been demonstrated that the convective assembly method can be used for deposition of cells,[38] and the related "drawdown method" has been used to deposit cells and particles in unpatterned centimeter-scale patches on a substrate.[39]

The process of convective assembly of two-dimensional colloidal crystals begins when the contact line of a receding liquid surface pins and the thin liquid film becomes thinner than the diameter of the particles. The menisci formed around the particles give rise to attractive capillary forces, and as the liquid evaporates, the particles are pulled together to form two-dimensional crystal nuclei.[1−3] A flux of liquid from the bulk of the suspension to the drying front of the crystal compensates for the fluid loss due to evaporation, which results in convective transport of particles to the drying front, propagating the crystal growth.[1,2] A mass balance allows to correlate the crystal growth rate, v_c, to the evaporation rate and particle volume fraction:

$$v_c = \frac{\beta j_e l \phi}{h(1-\varepsilon)(1-\phi)}$$

where β is an interaction parameter, j_e is the rate of evaporation, l is the drying length, ϕ is the volume fraction of the particles in suspension, h is the height of the deposited colloidal crystal, and ε is the porosity of the crystal.[3,4]

Prevo and Velev reported a modified convective assembly method that allows rapid and controllable deposition of particulate coatings from miniscule volumes of suspension.[6] A small liquid body containing particles at high volume fraction is trapped between two plates, and a linear motor pushes the top plate along the long axis of the bottom plate, thereby dragging the meniscus with it. Formation of the colloidal crystal occurs in a thin film on the bottom plate by conventional convective assembly. The use of a high volume fraction of particles serves to drastically decrease both the volume of the suspension and the time necessary for deposition of the colloidal crystal.[6]

We report here how a modification of the above method for convective assembly at a high volume fraction can be used to deposit rapidly close-packed yeast cell coatings on glass plates. We test the method by depositing *Saccharomyces cerevisiae* yeast cells, which are one of the most robust and intensively studied eukaryotic model organisms in cell biology and biotechnology. The cells are much larger than the other types of particles deposited previously using this method, which affects the deposition process by the presence of sedimentation. The goals of this study are to investigate the fundamentals of the effect of cell size on the deposition process and develop means of controlling of the convective assembly procedure to obtain large uniform coatings. We first present a model simulating the cell deposition process that allows identifying the conditions that control the coating uniformity. We then investigate the effect of these parameters on the deposition of coatings from cells and mixed cells and particles.

Materials and Methods

Preparation and Characterization of Yeast Cell Suspension. A 10 wt % suspension of yeast cells was prepared by dispersing 0.5 g of Fleischmann's active dry baker's yeast, *Saccharomyces cerevisiae* (ACH Food Companies, Memphis, TN), in 4500 μL of deionized water obtained from a RiOs 16 reverse-osmosis water purification system (Millipore Corporation, Bedford, MA). The yeast cells were sprinkled over the room temperature water and allowed to reside for 5 min. The vial was then manually agitated to suspend the yeast cells in the water and was allowed to sit for 30 min. Following the cell hydration, 0.25 g of anhydrous dextrose (Fisher Scientific Chemical Division, Fair Lawn, NJ) was added to the suspension.

The pH of the suspension was measured using a compact pH meter (HORIBA Instruments, Irvine, CA) and was adjusted to 8.0 using cell culture tested 1.0 N NaOH (Sigma-Aldrich, St. Louis, MO). The pH was then adjusted every 30−45 min for several hours using small aliquots of NaOH until it stabilized at 8.0. Immediately prior to deposition, the cell suspension was sonicated gently (Branson Ultrasonics Corporation, Danbury, CT) for 15−20 s to break up aggregates.

The cell dispersions showed some degree of aggregation as the cells resist changes in the pH of the suspension away from the isoelectric point of 4 because of the −COOH groups and the other protonated macromolecules on their surface. The aggregation state of the yeast cells in these suspensions was determined by optical microscopy. Following 20 s of sonication, samples of the suspensions were taken prior to and following pH adjustment (i.e., at a pH of ∼4.3 and of ∼8.2). Ten microliters of the suspension was diluted in 500 μL of deionized water, mounted on microscope slides, and digitally photographed using an Olympus BX61 optical microscope. The percentage of aggregated cells was decreased both by the sonication and by repeatedly adjusting the pH of the suspension away from the isoelectric point, resulting in less than 25% of the cells being in aggregates.

Deposition of Cell Coatings. Fisherbrand 25 mm × 75 mm glass microscope slides (Fisher Scientific) were cleaned by overnight immersion in a Nochromix solution (Godax Laboratories, Cabin John, MD). The slides were carefully rinsed with deionized water and dried in an oven at 70 °C for 45 min. Two clean glass slides were attached to the deposition device. It was important that the edge of the top slide lie flat on the bottom slide to ensure the formation of a uniform meniscus. A volume of 12 μL from the cell suspension was then injected between the two slides and spread to form a uniform meniscus. The linear motor pushing the top slide was operated at 21.1 μm/s, while the cells were deposited onto the substrate in 15−45 min. The suspension was deposited at the ambient laboratory temperature of 22 ± 2.5 °C, and an ambient relative humidity of the laboratory ranging from 30% to 60%.

Coating Characterization and Modeling. To determine the uniformity of an entire coating, images were taken using a low-magnification Olympus SZ61 microscope equipped with a digital camera. An Olympus BX61 microscope with a CCD camera and 5× to 50× objectives were used for collecting high-magnification images of the cell structure using bright field, phase contrast, or oblique lighting. Images of the coatings were analyzed using digital image processing. Adobe Photoshop 7.0.1 was used in to measure the surface fraction of the cell coverage and the uniformity of the layers. A Leica TCS SPI laser scanning confocal workstation attached to a Leica IMBE inverted microscope with a Hamamatsu cooled color CCD was used to collect Z-stacks of images for three-dimensional rendering of the coatings. Active dried *S. cerevisiae* from MP Biomedicals (Solon, OH) was used for confocal imaging because the cells are fluorescent. A 488 nm Argon laser was used to view coatings with a 40× oil immersion objective. The various deposition

(34) Singhvi, R.; Kumar, A.; Lopez, G. P.; Stephanopoulos, G. N.; Wang, D. I. C.; Whitesides, G. M.; Ingber, D. E. *Science* **1994**, *264*, 696–698.
(35) Chen, C. S.; Mrksich, M.; Huang, S.; Whitesides, G. M.; Ingber, D. E. *Science* **1997**, *276*, 1425–1428.
(36) Folch, A.; Toner, M. *Biotechnol. Prog.* **1998**, *14*, 388–392.
(37) Ostuni, E.; Kane, R.; Chen, C. S.; Ingber, D. E.; Whitesides, G. M. *Langmuir* **2000**, *16*, 7811–7819.
(38) Kahraman, M.; Yazici, M. M.; Sahin, F.; Culha, M. *Langmuir* **2008**, *24*, 894–901.
(39) Lyngberg, O. K.; Thiagarajan, V.; Stemke, D. J.; Schottel, J. L.; Scriven, L. E.; Flickinger, M. C. *Biotechnol. Bioeng.* **1999**, *62*, 44–55.

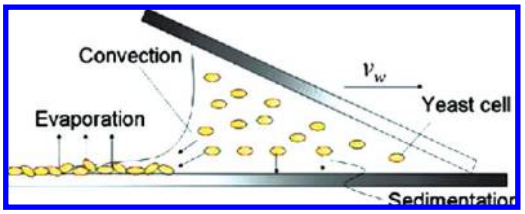

Figure 1. Schematic of the convective-sedimentation assembly process. The bottom slide remains in place while the top slide is translated to the right by a linear motor at a rate, v_w. Sedimentation, evaporation, and convection act on the cells during the deposition process.

mechanisms at work during convective-sedimentation assembly were modeled using Maple 9.00.

Deposition of Mixed Yeast Cell−latex Coatings. The yeast cell suspension for mixed coatings was prepared as described above. Sulfate latex microspheres (10 μm) (Interfacial Dynamics Corporation, Eugene, OR) were washed and concentrated using a Fisher Marathon micro A microcentrifuge (2700 *g* for 5 min). The two suspensions were mixed in a proportion such that the number of cells in the suspension would approximately equal the number of particles. The combined suspension was sonicated to reduce cell aggregation before deposition. The suspension was injected between the slides and deposited with the device at a forward inclination of 30°. To confirm the viability of the yeast cells, FUN 1 cell stain (Molecular Probes, Eugene, OR) was incubated with the cells for 30 min in a final concentration of 20 μM. The cells were then viewed in the fluorescence microscopy mode of the BX61. The live, vital cells metabolized the dye, and thus were no longer uniformly fluorescent.

Results and Discussion

The process of assembly of cells by convective evaporation is different from the assembly processes of conventional colloid particles because the morphology of cells is variable, they can interact in dense suspensions, and the size of the cells used in this study was an order of magnitude or more larger than the particles previously deposited using this method (12 nm to 1 μm).[6−8,10] The greater tendency toward sedimentation turned out to be a major factor affecting the process and specifically the uniformity of the coatings. In order to understand the effect of these factors and design processes, where the cells can be deposited with maximal efficiency and uniform thickness, we performed numerical evaluation of the parameters affecting the deposition process and their effect on the coating uniformity.

The sedimentation rate, V_s, of the large particles was estimated using the Stokes equation:[40]

$$V_s = \frac{2r_{cell}^2(\rho_{cell} - \rho_{susp})g}{9\mu_{susp}}$$

where r_{cell} is the radius of a cell, ρ_{cell} is the density of a cell, ρ_{susp} is the density of the suspension media, g is gravitational acceleration, and μ_{susp} is the viscosity of the suspension. The major assumption in the Stokes equation is that the particles are noninteracting hard spheres in a diluted suspension. The concentration of yeast cells in the suspensions being deposited in our experiments, however, is relatively high at 10 wt %. The viscosity of the suspension was adjusted to account for the high concentration of particles based on literature data for the relative viscosity

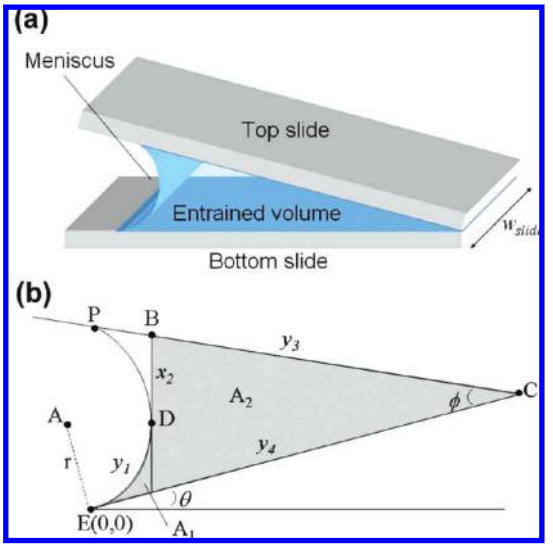

Figure 2. (a) Three-dimensional drawing of the physical system, with the position and shape of the meniscus. (b) Definition of the geometrical parameters used in the deposition model.

versus concentration of yeast cells[41] (the relative viscosity of our suspension was 1.4). The sedimentation rate of the cells in the suspension may also differ from the Stokes rate because of cell−cell interactions; at the experimental pH, the cell surfaces are negatively charged as a result of the presence of carboxyl and phosphate groups, so electrostatic repulsion forces predo minate.[42,43]

The sedimentation rate of the cells estimated from the Stokes equation was 1.16 μm/s. This is nearly 10% of the withdrawal speed, which was maintained at 21.1 μm/s for all experiments, while depositing a coating of length from 10 mm to 25 mm. Clearly, a significant amount of the cells in the liquid meniscus will sediment on the bottom slide during coating deposition. Thus, we define "convective-sedimentation assembly" as the process of depositing large particles or cells by evaporative convective assembly in the presence of sedimentation (Figure 1). The process involves a combination of multiple effects and complex particle transfer and deposition mechanisms. We developed a computational procedure that takes into account the effects involved and simulates the deposition process. The procedure and the results of the calculations are described below.

Convective-Sedimentation Deposition Model. *System Geometry*. The deposition takes place at the edge of a long meniscus of water trapped between two plates. The geometry is translationally invariable in the meniscus direction, and there is no redistribution of material parallel to the meniscus edge. Neglecting the effects of the two sides, which only slightly affect the deposition at the edges of the plates, we consider a slice with a width of a single cell diameter perpendicular to the edge. Because the plates in the experiments are hydrophilized, the water−glass contact angle was assumed to be ~0°. The meniscus of the entrained liquid was assumed to be cylindrical[44] and tangent to both plates (Figure 2a). To test the validity of this assumption, we calculated the Bond

(40) Russel, W. B.; Saville, D. A.; Schowalter, W. R. *Colloidal Dispersions*; Cambridge University Press: Cambridge, U.K., 1989.

(41) Aiba, S.; Kitai, S.; Ishida, N. *J. Gen. Appl. Microbiol.* **1962**, *8*, 103–108.
(42) Ahimou, F.; Denis, F. A.; Touhami, A.; Dufrene, Y. F. *Langmuir* **2002**, *18*, 9937–9941.
(43) Tazhibaeva, S. M.; Musabekov, K. B.; Orazymbetova, A. B.; Zhubanova, A. A. *Colloid J.* **2003**, *65*, 132–135.
(44) Hunter, R. J. *Foundations of Colloid Science*; Clarendon Press: Oxford, 1987.

number, which is the ratio of gravitational forces to surface tension:

$$\mathrm{Bo} = \frac{\rho g r^2}{\sigma}$$

where ρ is the density of the suspension media, g is gravitational acceleration, r is the characteristic length, and σ is the surface tension. The characteristic length could be either the radius or the diameter of the meniscus. Thus, the estimated Bond number is between 0.2 and 0.3, indicating that surface tension predominates,[45] so the assumption that the meniscus is cylindrical is reasonable. The meniscus geometry is then described by a system of four equations, the parameters of which are defined in Figure 2b.

$$y_1 = -\sqrt{r^2 - (x - a_x)^2} + a_y$$

$$x_2 = d_x$$

$$y_3 = (c_x - x)\tan(\phi + \theta)$$

$$y_4 = -x\tan\theta + e_y$$

The experimentally variable parameters are the angle between the two plates, ϕ, and the angle of the bottom plate with the horizontal, θ. These two angles, together with the volume of the liquid body, define the geometry of the system (Figure 2b). To calculate the values of all parameters, an initial estimate of the radius of the meniscus was made based on the known physical parameters of the system. This radius was used to determine the initial locations of points A, B, C, D, E, and P, as well as the lines y_1, x_2, y_3, and y_4. The set of simplified equations ignores the unshaded area in Figure 2b, but this small volume may not significantly affect the results.

The target function in the iterative procedure for calculating the exact radius of curvature and meniscus shape was the side area of the slice, A_{sys}. It was determined independently by dividing the entrained volume by the width of the slide w_{slide}. The surface area was also calculated by integration over the shaded areas A_1 and A_2 in Figure 2b: $A_1 = \int_0^{D_x(y_1)}(x) - y_4(x))\mathrm{d}x$ and $A_2 = \int_{D_x}^{C_x(y_3)}(x) - y_4(x))\mathrm{d}x$. The value of the radius, r, was varied until $(A_1 + A_2)$ became equal to A_{sys}.

Model Components and Assumptions. Several assumptions were made to simplify the calculations. The cells were assumed to be spherical and well-dispersed particles of uniform density. The evaporation rate was assumed to be constant over the entire deposition time span and over the surface of the meniscus, while the evaporation from the exposed sides of the entrained volume was neglected.

The process included three distinct mechanisms for cell redistribution: convection, sedimentation, and evaporation. The convection and evaporation components of the model

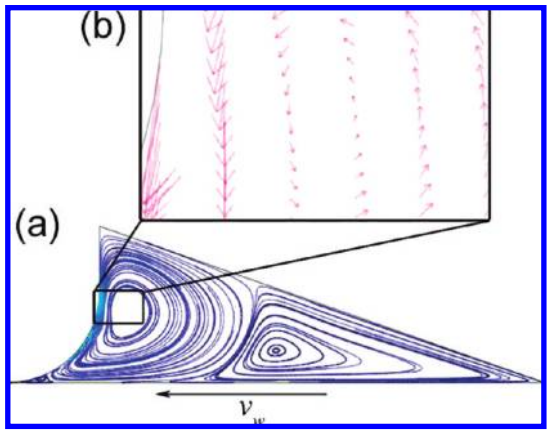

Figure 3. FEMLAB simulation of the fluid flow within the entrained volume: (a) streamlines of the flow; (b) velocity vectors showing circulation near the meniscus. The size of the arrows indicates relative magnitude of the vectors.

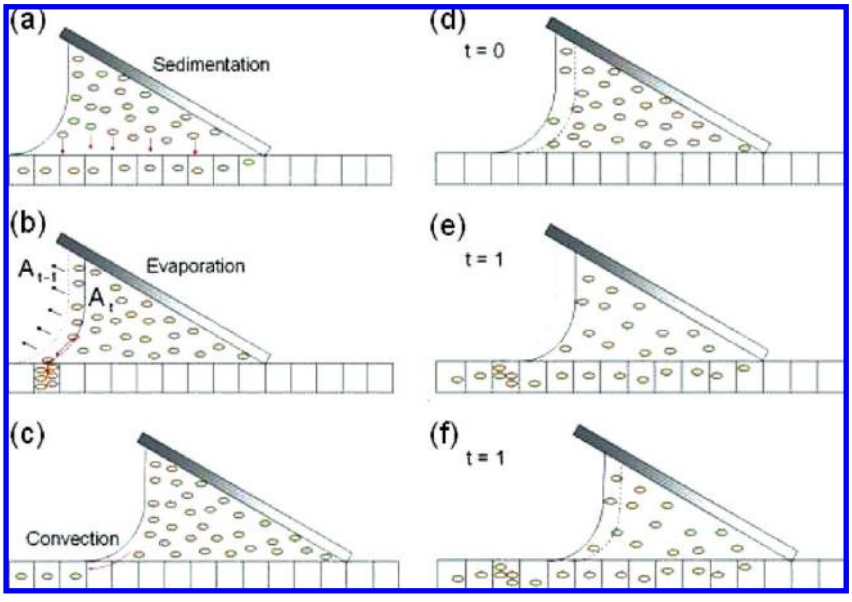

Figure 4. (a–c) Illustration of the algorithms taking into account the three deposition mechanisms: (a) *sedimentation*, where the cells drop straight down onto the plate; (b) *evaporation*, during which the cells in the evaporating portion of the entrained volume, $A_{t-1} - A_t$, are deposited in the bin directly under the meniscus; and (c) *convection*, in which cells are pulled into the thin film in front of the meniscus and are deposited there. (d–f) Schematic sequence of the algorithm of the combined three-mechanism model: (d) Initial condition of the entrained volume and the array representing the bottom plate. The decreased meniscus volume following evaporation is indicated by the dashed line. (e) Time has increased by a single interval, evaporation has occurred, and cells have been deposited. (f) The bottom array has advanced, corresponding to the moving of the top slide and thus the meniscus. The bin width in all frames has been increased for ease of visualization.

describe the action of convective assembly, where the cells were pulled forward and then deposited at the front of the meniscus. In order to account for the sedimentation component, we also had to consider the effect of the liquid flow mixing and recirculation opposing the sedimentation, which would otherwise lead to a permanent vertical gradient in cell concentration. When we simulated cell deposition without any mixing in the liquid bulk, we obtained significant deviations from the experimental results. Further, simulations of the fluid flow in the liquid body demonstrated that a significant degree of fluid mixing and recirculation within the entrained volume was present as a result of the mechanical withdrawal of the meniscus and the convection of fluid caused by evaporation. To evaluate the impact of the circulation, basic modeling of the flows in the system was completed using FEMLAB. The simulation took into account the evaporation of the liquid and the movement of the bottom plate with regard to the meniscus but without cells in the entrained volume.

The streamlines of the simulated flow plotted in Figure 3 demonstrate that mixing occurs within the entrained volume, with the highest rates at the meniscus. The velocity vectors in the inset show a large vortex near the meniscus and decreasing velocity away from the meniscus. When the sedimentation rate was compared to the value of the velocity field at a height of 10 μm along the length of the entrained volume, the sedimentation rate exceeded the velocity field for 28% of the entrained volume. Thus, the velocity of the fluid appears high enough to keep the cells well mixed in most of the fluid volume. Only the particles within two cell diameters of the surface were affected by sedimentation; the cells in the bulk of the entrained volume were well mixed at all times. Thus, in the subsequent modeling, the concentration of cells within the entrained volume was kept uniform at all times.

Algorithm of the Simulation. The simulation algorithm calculated the number of cells deposited at any given moment on the bottom slide below the moving meniscus. The bottom surface is split into an array of "bins" into which the cells are deposited (Figure 4a,d). Each bin in the array has a width equal to one cell diameter. The meniscus motion is modeled by moving at each time interval the bottom surface, with the array's bins, relative to the entrained volume. The array was shifted to the left at time intervals, t, based on the withdrawal speed, v_w, and the bin width: $t = 2r_{cell}/v_w$. The movement of the bottom slide served to simplify the calculations and was physically equivalent to the motion of the top slide with the attached meniscus in the experiments. Since the system is well mixed, the total number of cells in the entrained volume was decreased by the number of cells deposited in the bins at each time increment following the algorithms describing the three deposition mechanisms (see below). The time then advanced one unit, and the array index increased by one. Before the next step, the entrained volume was decreased proportionally to the evaporation rate, and the geometry of the entrained volume was recalculated. The entire procedure continued iteratively until either no cells remained or the entrained volume had been entirely evaporated (Figure 4).

Sedimentation Algorithm. The FEMLAB modeling of fluid velocity points out that the particles remain uniformly distributed in the bulk of the entrained volume until they approach the substrate. The height from which cells will sediment onto the substrate was calculated using the Stokes sedimentation rate as $h = V_s t$. All cells contained in the boundary layer of height h will be deposited onto the substrate (Figure 4a). The number of cells landing into each bin in a time interval, t, can then be determined as the deposition flux:

$$n_{sediment,bin} = \frac{nhl_{volume}}{A_{int} z_{sediment}}$$

where n is the number of cells in the bulk, l_{volume} is the length of the entrained volume, and $z_{sediment}$ is the number of bins under the entrained volume. The cells that had sedimented were divided evenly among the bins currently under the entrained volume. The primary parameters used in the numerical evaluation of the sedimentation are listed in Table 1.

Table 1. Summary of the Primary Parameters Used in the Calculations

symbol	equation	denoted parameter
	Sedimentation	
V_s	$V_s = \frac{2r_{cell}^2(\rho_{cell}-\rho_{susp})g}{9\mu_{susp}}$	sedimentation rate
t	$t = \frac{2r_{cell}}{v_w}$	time step for progression of the array
h	$h = V_s t$	height from which sedimentation occurs
$z_{sediment}$	$z_{sediment} = \frac{l_{volume}}{d_{cell}}$	number of bins under entrained volume into which sedimentation occurs
$n_{sediment,bin}$	$n_{sediment,\,bin} = \frac{nhl_{volume}}{A_{int} z_{sediment}}$	deposition flux due to sedimentation
	Evaporation	
J_e		evaporation flux
n_{evap}	$n_{evap} = n\frac{A_{t-1}-A_t}{A_{t-1}}$	deposition flux due to evaporation
	Convection	
L_{film}	$L_{film} = \frac{v_w d_{cell}(1-\varepsilon)(1-c_i)}{\beta j_e c_i}$	length of the thin film in which convection occurs
N_{film}	$N_{film} = \frac{v_w d_{cell}^2(1-\varepsilon)}{V_{cell} w_{slide}}$	number of cells deposited by convection at a given time
z_{conv}	if $z_{conv} < 200$, $z_{conv} = \frac{L_{film}}{d_{cell}}$ else $z_{conv} = 200$	number of bins in the thin film
n_{conv}	$n_{conv} = \frac{N_{film} t}{z}$	deposition flux due to convection

Evaporation Algorithm. The evaporation rate was assumed to be constant for the entire deposition process and over the entire meniscus. As the liquid evaporated, the entrained volume decreased, and thus its geometry had to be recalculated. The numerical relationship between the radius of curvature, r, and the entrained volume, V, plotted in Figure 5, could be approximated well by $r = aV^{0.5}$, where a varies from 0.06 to 0.14, depending on the values of θ and ϕ. Keeping in mind that the entrained volume is the area, A_{int}, multiplied by the width of the slide, it is reasonable that V would decrease with r^2. This relationship was used to determine r at each volume instead of recalculating it using the iterative procedure described above.

In addition to decreasing the entrained volume, evaporation also results in the collection and deposition of the cells in the vicinity of the meniscus. To simulate this effect, the cells collected at the air−water meniscus are deposited into the bin directly below it (Figure 4b). The number of cells deposited by evaporation is calculated by the change in the area of the

(45) Princen, H. M. In *Surface and Colloid Science*; Matijević, E., Ed.; Wiley-Interscience: New York, 1969; Vol. 2, pp 1−84.

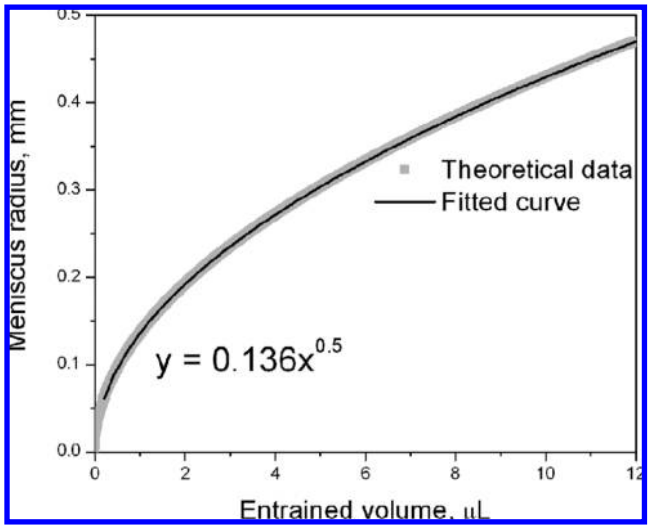

Figure 5. Relationship between the meniscus radius and the entrained volume as evaporation progresses. The fitting equation and parameters are included in the plot.

(single slice of the) entrained volume. The deposition flux at a given time, t, is $n_{evap} = n[(A_{t-1} - A_t)/A_{t-1}]$, where the parameters used are defined in Table 1.

Convection Algorithm. Convection, which drags the cells inside the film to the end of the meniscus for deposition in a close-packed layer, has a significant effect on the structure of the coating. This is modeled by distributing the cells deposited by convection into the bins at the edge of the meniscus where a thin liquid film is formed in the actual system (Figure 4c).

The material flux balance first derived by Dimitrov and Nagayama,[4] modified for the cell system, defines the length of the thin film in which deposition by convection occurs:

$$L_{film} = \frac{v_w d_{cell}(1-\varepsilon)(1-c_i)}{\beta j_e c_i}$$

where ε is the porosity of the cell layer, c_i is the concentration of the bulk suspension at that particular time, β is the coefficient of proportionality that depends on particle−particle and particle−substrate interactions (varies from 0 to 1 being highest for noninteracting particles in dilute suspensions), and j_e is the evaporation flux. The value of ε was determined from the initial layer thickness measured from experimental data where sedimentation did not yet affect the coating. The value of the coefficient of proportionality, β, was chosen empirically as 0.5, reflecting that the large yeast cells have high friction with the substrate and that the suspension was highly concentrated.

The particle flux is described by two equations: $h_f j_p = v_c h(1-\varepsilon)$ and $j_p = N_p V_p v_p$, where h_f is the liquid film thickness, j_p is the particle flux, v_c is the rate of crystal growth, h is the height of the particle layer, N_p is the number of particles per unit volume, V_p is the volume of one particle, and v_p is the macroscopic mean velocity of the suspended particles.[4] By combining these two equations we obtain:

$$h_f N_p v_p = \frac{v_c h(1-\varepsilon)}{V_p}$$

It is difficult to determine v_p experimentally, so a new variable, N_{film}, was defined as the total number of particles deposited in the thin film per unit of time:

$$\frac{N_{film}}{h^2} = N_p v_p$$

Since the deposition process occurs at steady state, $v_c = v_w$, it is also reasonable to assume that $h_f \approx h$. The thickness of the layer, h, for this situation is the diameter of one cell. Combining all above, we arrive at the following equation for the balance in a one-cell-thick slice of the meniscus:

$$N_{film} = \frac{v_w d_{cell}^2(1-\varepsilon)}{V_{cell} w_{slide}}$$

The value of N_{film} remains constant for the entire deposition process, but the value of L_{film} changes with the concentration, c_i. The number of bins that L_{film} consists of, z_{conv}, is calculated by dividing L_{film} by the cell diameter. Thus, the deposition flux was calculated as follows:

$$n_{conv} = \frac{N_{film} t}{z_{conv}}$$

The number of bins, z_{conv}, increases rapidly as the concentration decreases, as the balance points out that the length of the film is inversely related to the particle concentration. Extremely high values for the film length are not physically realistic, as too long films will break and dewet. A value of $z_{conv} = 200$ was set as the maximum number of bins, allowing a maximum drying length of 1000 μm, a reasonable value considering reported values of 1400−2600 μm for latex particles.[6] For $z_{conv} < 200$, the calculated number of cells, n_{conv}, is placed into z_{conv} bins directly in front of the meniscus. For $z_{conv} > 200$, n_{conv} is placed into only the first 200 bins in front of the meniscus. The parameters used to calculate the convection are listed in Table 1.

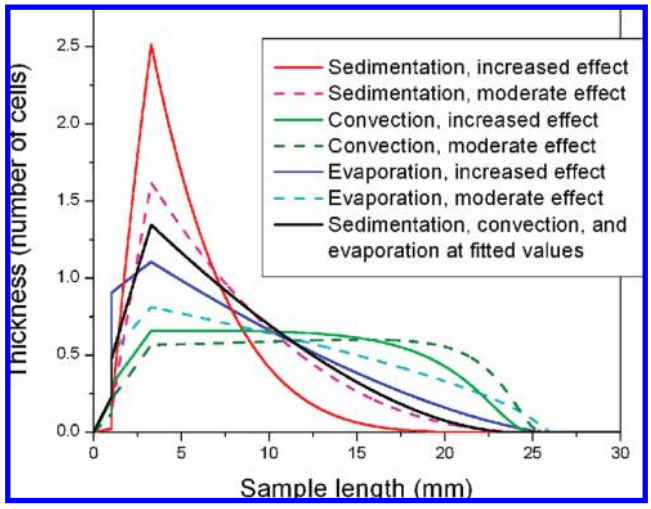

Figure 6. Simulated effect of the processes taking place during the deposition on the coating. When sedimentation is the leading effect, a sharp peak is seen in the profile; as the effect of sedimentation is decreased, the peak shortens, improving the coating uniformity. When convection is the primary effect, the coating is relatively flat and uniform, and as the effect is decreased, a small peak appears at the end side of the coating. For evaporation as the primary effect, a small peak is present, and as the effect is decreased, the peak shortens, improving the coating uniformity. A fit of a real experimental profile is included in black for comparison.

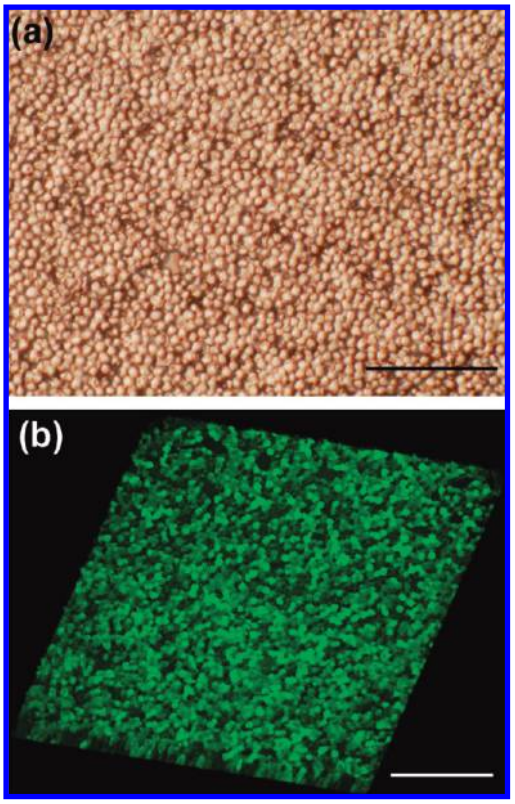

Figure 7. (a) Optical micrograph of a nearly complete monolayer of yeast cells. (b) Three-dimensional rendering of a dense yeast cell coating using confocal microscopy. A few cells deposited in a second layer are observed. Both scale bars are 50 μm.

Model Component Analysis. The convection, evaporation, and sedimentation mechanisms affect the deposition process and the uniformity of the coating in different ways. To evaluate how the interplay of the deposition mechanisms affects the uniformity of the coating, the effect of each mechanism on a profile was evaluated individually. The results of this analysis are plotted in Figure 6.

When convection is the primary deposition mechanism, the coating thickness is nearly constant, which is exactly the case for all our earlier studies with microparticles[6] and nanoparticles.[7,10] Decreasing the rate of convection does not significantly change the coating profile because a small number of cells is spread thinly over a uniform number of bins for the majority of the coating. When sedimentation is the primary effect, the peak is very high, and the profile has a very steep slope. However, if the effect of sedimentation is decreased while still keeping it the primary component, the curve levels out, and the peak drops down significantly because a larger number of cells are deposited into an increasing number of bins at each time.

When the deposition flux due to evaporation is the primary effect, a lower peak results, leading to a coating that closely resembles the profile fitted to the experimental data. When the effect of evaporation on the deposition flux is decreased to a moderate value, the height of the peak drops, and the direction of curvature of the profile changes. The uniformity of the coating thereby improves. For large spheres, coating quality has been found to increase with an increase in the evaporation rate.[46] However, in Figure 6, evaporation refers only to the deposition flux due to evaporation; the evaporation rate itself is not changed. From our analysis, we can see that a lower sedimentation rate and fewer cells deposited by evaporation would result in a more uniform coating, which could be accomplished by changing the suspending media and increasing the deposition rate to increase the effect of the vortex.

(46) Kitaev, V.; Ozen, G. A. *Adv. Mater*. **2003**, *15*, 75–78.

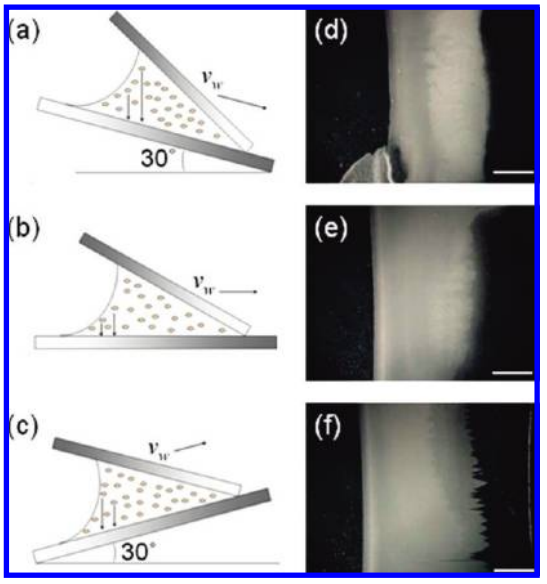

Figure 8. Examples of the effect of device inclination on the coating uniformity. (a−c) Schematics of device alignment at (a) backward inclination, (b) no inclination, and (c) forward inclination. (d−f) Micrographs of coatings deposited at the corresponding inclinations. All scale bars are 5 mm.

Convective-Sedimentation Deposition. The experimental deposition of large-scale cell layers matched the expectations of the simulation. The cell coatings were near single layer and uniform throughout most of their middle section. An example of a coating from cells deposited by convective-sedimentation assembly is shown in Figure 7a. A three-dimensional rendering of a coating structure observed by confocal microscopy is presented in Figure 7b. The images collected in the Z-stacks showed that the majority of the cells were within 5 μm of the surface, and the remainder were within 10 μm of the surface, indicating that the cell coating is packed mostly into a single layer. Dispersed islands of cells in a second layer are seen in several locations as bright spots.

The sedimentation process concurrent to the convective assembly likely resulted in thickening of the layer of deposited cells. It appears that sedimentation causes the coatings deposited to be of nonuniform density overall because more cells have sedimented onto the layer at the back end of the coating than at the front edge. The change in the thickness of the layer becomes observable partway along the length of the coating (Figure 8d−f).

One way to affect the sedimentation and potentially to improve the uniformity of the coating is to incline the deposition setup and thus change the trajectories of the settling cells. Inclining the entire device should change the point at which the coating thickness changes, assuming that mixing within the meniscus does not significantly change the direction of sedimentation from the vertical. By moving that point of thickness change to the front of the coating, the uniformity of the coating should improve, while moving this point backward should decrease the uniformity. To test this hypothesis, the effect of sedimentation direction and of inclination of the deposition device on the coating uniformity was investi-

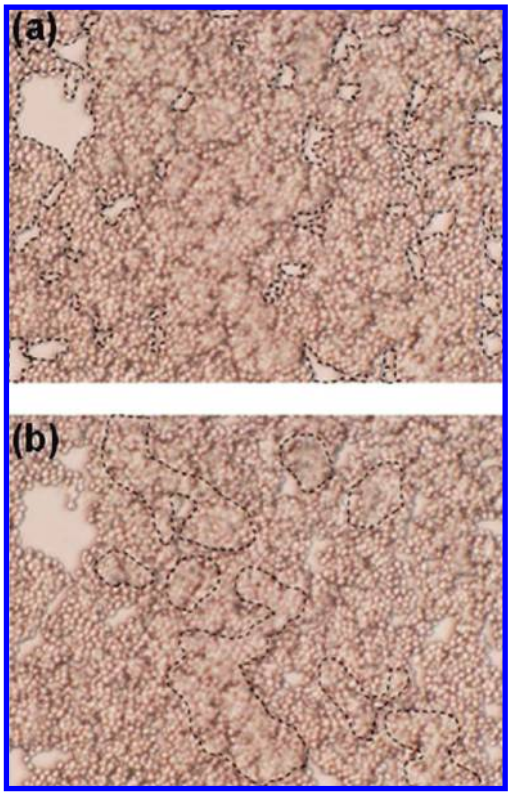

Figure 9. Illustration of the image analysis of a cell coating for development of a thickness profile. (a) Selection of areas (dotted lines) of the image without cells. (b) Selection of areas of the image with two layers of cells.

gated. The device was inclined backward (Figure 8a), in which case the cells sediment farther down the coating, and thus away from the meniscus, and forward (Figure 8c), in which case the cells sediment toward the meniscus. The device was angled in both forward and backward inclinations and the resulting coatings were examined by microscopy.

In Figure 8d−f, the coating begins on the left, with thinner layers being darker. The coatings thicken as deposition progresses. The transition from thinner to thicker coatings is abrupt, defining the point at which the sedimentation begins to contribute strongly to the thickness. This abrupt thickness change was confirmed using higher magnification optical microscopy. The inclination has a significant effect on uniformity. The coating deposited with backward inclination (Figure 8d) has a small, uniformly thin area followed by a larger, uniformly thick area. The coating deposited at no inclination (Figure 8e) has a small, uniformly thin area where deposition was initiated; it then thickens, but the thickness varies over the length of the sample, as shown by the color variations. The coating deposited at forward inclination (Figure 8f) has a very small thin area, followed by a large, uniform thick area that thins as the liquid meniscus runs out of material. As expected, depositing the coating by inclining the device forward improved its uniformity, because the thickness increased at an earlier point on the coating. Backward inclination, which causes thickening at a point farther along the deposit, decreased the uniformity of the coating. The effect of the inclination angle on the uniformity of the cell films is modeled and analyzed quantitatively in the next sections.

Parametric Experiments and Model Evaluation. It is difficult to suppress the cell sedimentation, so two additional experimental parameters were varied independently to optimize

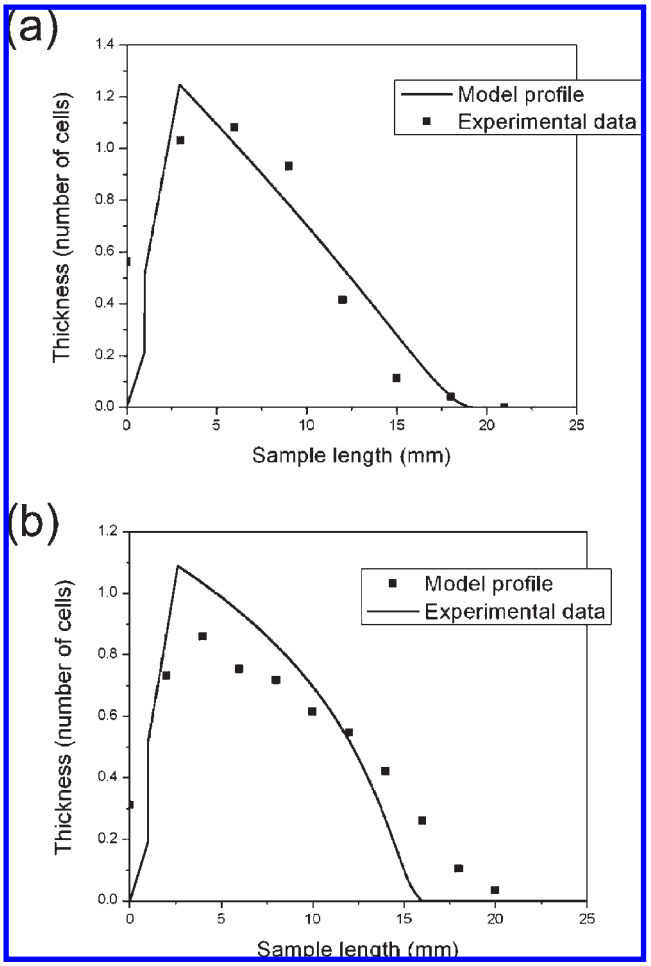

Figure 10. Comparison of simulated profiles with experimental data illustrating the accuracy of the model. (a) Experimental data from a θ variation experiment, where $\theta = 0°$. (b) Experimental data from a ϕ variation experiment, where $\phi = 29°$, with a forward inclination of 20°.

the convective-sedimentation deposition process and to assess the predictive capability of the model. These parameters were θ, the angle of the entire device, and ϕ, the angle between the two slides. As in the first experiments, a 10 wt % suspension of live yeast cells, adjusted to a pH of 8, was deposited at ambient temperature and relative humidity. Initially, θ was varied, and the results were used to fit the model to the data. The angles at which coatings were deposited were 59°, 45°, 20°, and 10°, both forward and backward, in addition to no inclination. For this experiment, ϕ was held constant at 19°.

The experiments in which ϕ was varied while θ was held constant were performed at both forward and backward inclinations of 20°. The angles of ϕ at which coatings were deposited were 11°, 17°, 23°, and 29°. This set of experiments was then used to determine how well the model fits the data from the ϕ variation based on the parameters from the θ fit. To reconstruct the profiles of the actual cell coatings, images of the plates with deposited layers were acquired and analyzed to determine the cell coverage and the uniformity of the layers. A grid pattern was used to obtain images over the entirety of the sample. At each position along the length of the substrate, three images were taken across the width of the sample. The nonuniform side edges of the deposited layer were not imaged, but the front and back ends of the deposited layer were imaged.

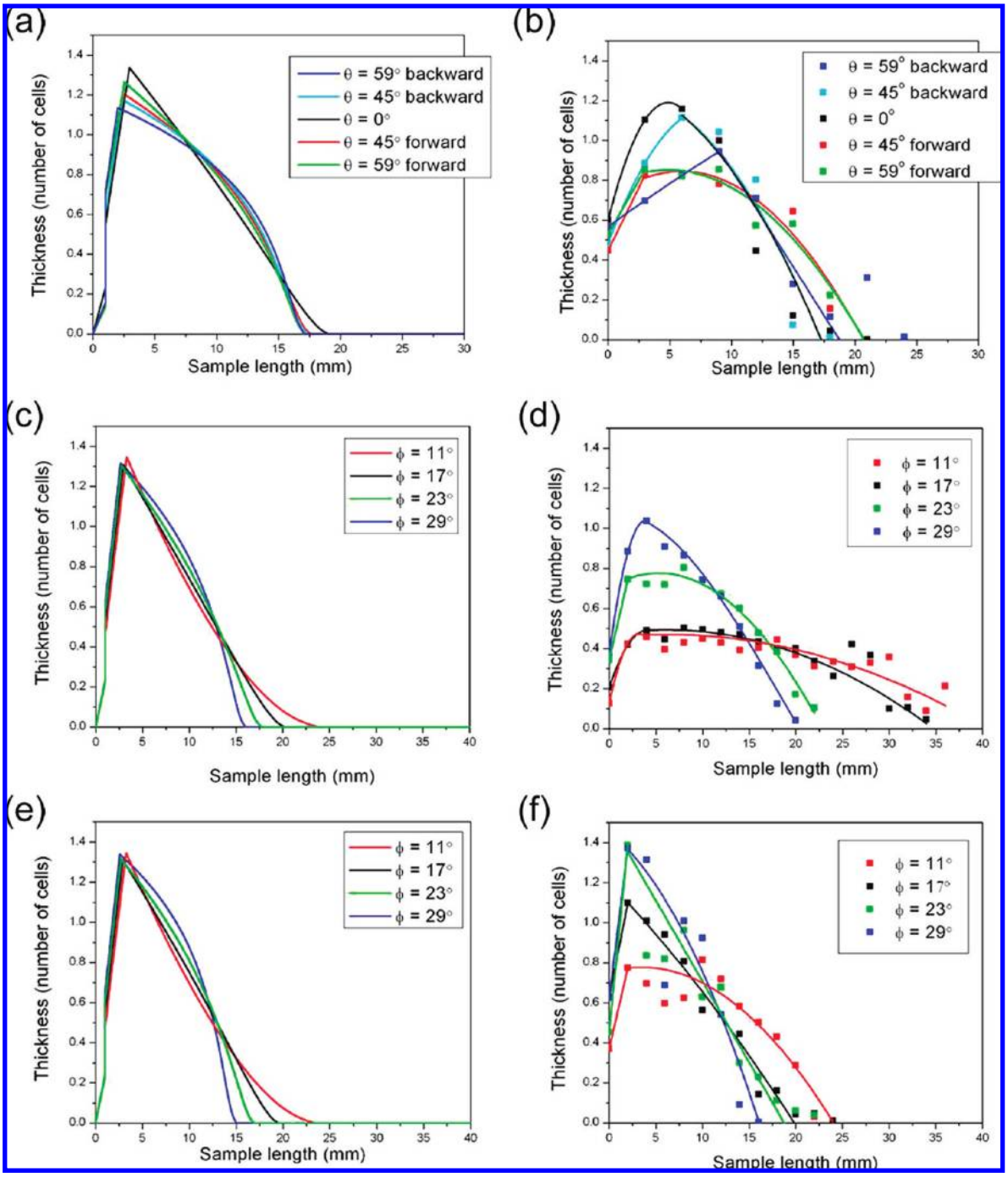

Figure 11. Coating thickness profiles from model and experimental data. (a) Model and (b) experiment profiles showing the effect of variation of θ. (c) Model and (d) experiment profiles showing the effect of variation of ϕ at a forward inclination of 20°. (e) Model and (f) experiment profiles showing the effect of variation of ϕ at a backward inclination of 20°. Lines in all experiment plots are to guide the eye.

The images collected were analyzed as follows. First, all of the areas in an image without cells were selected at one time (see Figure 9a), and the number of pixels was counted. Then, all the areas that were two cell layers thick were selected (see Figure 9b), and again the number of pixels was counted. The fraction of the area covered was determined from the total number of pixels in the image as follows:

$$\text{Fraction Covered} = \frac{N_{\text{Total}} - N_{\text{Empty}} + N_{2-\text{Layer}}}{N_{\text{Total}}}$$

where N is the number of pixels for the given condition. The coatings were no more than two cell layers thick. The fraction covered can be interpreted as the average thickness of the coating at that position. Thus, a fractional coverage of less than 1.0 would indicate an incomplete layer, and a value greater than 1.0 would indicate that a portion of the layer is two cells thick. These data were then used to plot the thickness of the coating as a function of the distance from the beginning.

Fitting and Model Accuracy. The results of the θ variation experiment were used to fit the model to the experimental data. The first fitting parameter was the evaporation flux. The fitted value of $J_e = 0.014$ μm/s is ~40% of the flux estimated in the earlier experiments with monodisperse latex particles.[6] This is a reasonable value for a parameter that is otherwise hard to

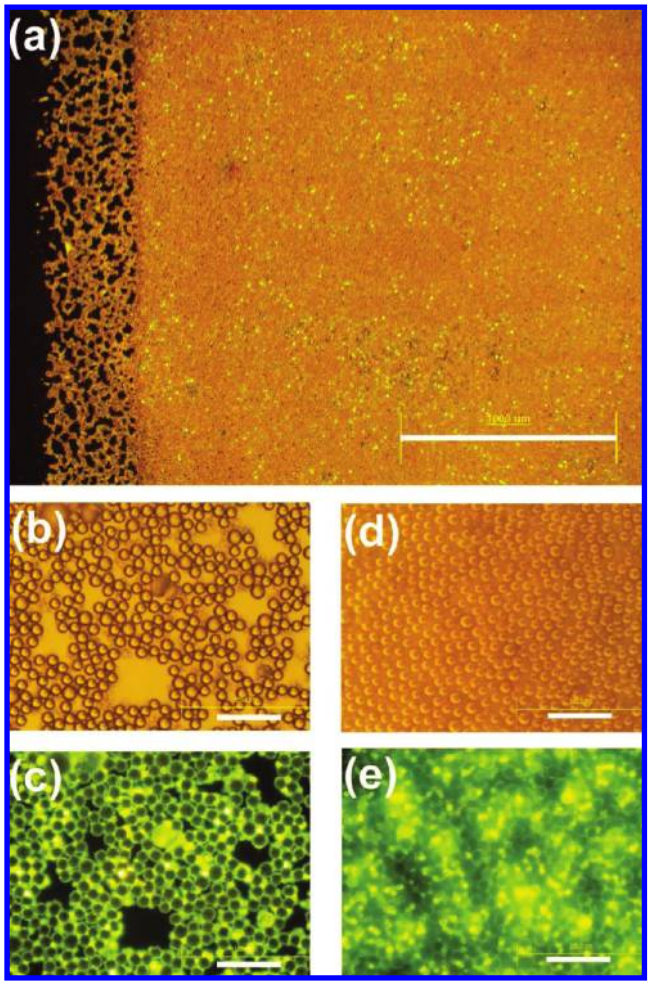

Figure 12. (a) Micrographs of a composite coating of particles and yeast cells. The cells are stained and fluoresced. (b,c) Submonolayer coating of yeast cells and particles. (c) Yeast cells cluster around the latex particles. (d,e) Complete monolayer coating of latex particles. Image (e) is taken from the bottom up and shows the collection of the yeast cells around the bottom part of the latex particles. The scale bar is 1000 μm for panel (a) and 50 μm for (b−e).

measure, as we expect evaporation from a thick dense layer of hydrated cells containing some proteins and buffers to be slowed with regards to the one from latex spheres in pure water. The second fitting parameter was the deposition flux, n_{evap}. We assumed in the model development that all cells in the vicinity of the meniscus would be carried by the flux in the drying film and deposited into the first bin under the meniscus. After fitting, we obtain that only 37.5% of the cells are deposited in the first bin, and the remainder are redispersed in the meniscus bulk. The redispersion can be correlated to the FEMLAB calculations that show a vortex near the meniscus, which would likely redistribute many of the cells entrained in the meniscus, decreasing the flux (Figure 3). The last fitting parameter was the sedimentation rate, V_s. This parameter needs fitting as the sedimentation of the cells in the thin boundary layer toward the substrate is likely slowed down by the proximity of the surface. The sedimentation rate was found to best match the experimental data at a fitted rate of 0.35 μm/s, which is ~1/3 of the calculated bulk value of 1.16 μm/s. This value agrees well with the literature. Since we are examining sedimentation close to a solid plane, the Stokes rate should be corrected for the additional dissipation in the thin liquid layer between the sphere and the surface. For yeast cells that should reach the surface in 1 s, based on the calculated rate of 1.16 μm/s, the center of the particle is 3.66 μm from the surface. Since the ratio of particle radius to distance of the particle center from the surface is 0.68, earlier theoretical studies point out that the rate should be decreased by a factor of ~3.036,[47] in excellent agreement with our fitted value.

Most of the lengths and thicknesses of the coatings calculated from the model are in good agreement with the experimentally determined profiles (Figure 10a). All θ variation profiles show that device inclination leads to more uniform coatings (Figure 11a−b). The data have higher variability than the model; however, the experiments show a greater dependence on θ than does the model. The experiments showed that forward inclination at high angles results in more uniform coatings. Additionally, the experiments showed that at backward inclination, the peak that results from sedimentation moves further back along the sample length. The model indicates that backward inclination leads to marginally more uniform coatings; however, these differences fall within the experimental error for the profiles.

At both forward and backward inclinations for ϕ variation, both data and model indicated that the coating length decreases and the coating thickness changes more rapidly as ϕ increases (Figure 11c−f). When the forward-inclined coatings are compared to the backward-inclined coatings, both model and experiment agree that the forward-inclined coatings are longer. At both inclination directions for 23° and 29°, the length and height of the coatings calculated using the model matches the experimental values. Additionally, the lengths of the backward-inclined coatings at 11° and 17° from the model match those from experiment, although their heights do not. For forward inclination, both the lengths and heights differ significantly. Even though the model does not fit well at low ϕ, we can draw the conclusion that, for each inclination direction, ϕ = 11° with forward inclination yields the most uniform coatings.

In summary, the model captures the key trends found in the experimental data but fails to describe quantitatively some of the profiles of the deposited coatings. Because the experiments were performed using a concentrated cell suspension, there are numerous effects such as the interactions between the cells and their partial aggregation that are hard to control and could affect the profiles of some of the coatings deposited. However, the results clearly point out how the conditions during the convective-sedimentation deposition can be adjusted so that live cell coatings can be deposited uniformly. Both the model and the experiments showed that increasing the angle θ results in more uniform coatings. The experimental data show that the coatings deposited at a forward inclination of 45° and 59° were the most uniform. Both the model and the experimental profiles indicated that decreasing the angle ϕ between the plates in both inclination directions improved the uniformity of the coating, with ϕ = 11° at forward inclination resulting in the most uniform coatings.

Codeposition of Yeast Cells and Large Particles. Cell coatings have a wide variety of potential applications, including bioreactor surface coatings, biosensors, gradient bioassays, cell signaling studies, toxicity studies, implant coatings, self-cleaning "artificial skin" and others. One of the specific advantages of the convective assembly is that it can be used to deposit any type of particles suspended in liquid,[48] which may

(47) Brenner, H. *Chem. Eng. Sci.* **1961**, *16*, 242–251.
(48) Prevo, B. G.; Kuncicky, D. M.; Velev, O. D. *Colloids Surf. A: Physicochem. Eng. Aspects* **2007**, *311*, 2–10.

include potentially a wide number of cell types in suspension. A potential problem of such coatings could be the low mechanical stability and poor abrasion resistance of the cell layers. One simple solution to this problem is to codeposit the cells together with a protective layer of particles.[49] A rudimentary system of this type was demonstrated by codepositing with the convective-sedimentation process mixed monolayers of yeast cells and large latex particles (10 μm). The large latex particles were used to create a porous covering that would provide protection from external perturbations for the yeast cells. Thus, the cells would be protected while still having access to nutrients and being able to proliferate through the coating of latex particles. The latex particles and yeast cells were mixed together prior to deposition. The amounts of the yeast cell suspension and the latex suspension that were used for the deposition were determined such that the number of yeast cells would be approximately equal to the number of latex particles. An example of such a composite coating is shown in Figure 12a.

During the deposition process, the yeast cells collected around the larger latex particles. This can best be seen in the thin section at the front of the sample in Figure 12b,c. The clustering of yeast cells around the bottom parts of the latex particle also occurs with multimodal colloidal particles and is known as *size-selective segregation*. The meniscus around the larger latex particles draws the smaller yeast cells closer via capillary forces.[50,51] When the sample thickens due to sedimentation, a complete monolayer of latex particles deposits on the top of the coating with yeast cells collected around the bases of the latex particles (Figure 12d,e).

To confirm the viability of the deposited cells, FUN 1 cell stain was added to a cell coating, which was then viewed to determine whether the dye had been metabolized. The presence of nonuniform fluorescence within the cells, where the dye was collected in the center of cell, confirmed that the cells were able to metabolize. Such coatings immersed in media where the cells could grow and divide may function as an "artificial skin," where debris and contaminants collected on the top layer of cells are sloughed off by external flows. As the bottom layer of cells is protected by the large latex particles, it may remain in place for regeneration of the top cell layer of the coating. By changing the type of cell used, additional functionality (e.g., contaminant digestion, antibacterial secretion) could be added to such coatings.

(49) Flickinger, M. C.; Schottel, J. L.; Bond, D. R.; Aksan, A.; Scriven, L. E. *Biotechnol. Prog*. **2007**, *23*, 2–17.
(50) Yamaki, M.; Higo, J.; Nagayama, K. *Langmuir* **1995**, *11*, 2975–2978.
(51) Kralchevsky, P. A.; Denkov, N. D. *Curr. Opin. Colloid Interface Sci*. **2001**, *6*, 383–401.

Conclusions

We investigated the deposition of live yeast cells and large particles using convective assembly. Sedimentation was found to significantly alter the uniformity of the coatings. A "convective-sedimentation" assembly method was developed for the rapid deposition of uniform, close-packed coatings of yeast cells. This method could also be used for the deposition of other suspensions of robust eukaryotic cells and large particles. A computational model of the deposition process helped in understanding the various mechanisms involved in the convective-sedimentation deposition process. Parametric experiments served the dual purpose of optimizing the deposition process and evaluating the computational model.

Several conclusions are clear from the investigation of the experimental and model profiles. The model approximates the experimental trends reasonably well at most conditions for variation of the angle of the deposition device, θ, and the angle between the two plates, ϕ. Both experiment and model indicated that large forward inclination, θ, along with small ϕ, yield more uniform coatings. The monolayer composite coatings of cells and particles have numerous potential applications, including bioreactor surface coatings, biosensors, gradient bioassays, cell signaling and toxicity studies, implant coatings, self-cleaning "artificial skin", and others.

Acknowledgment. This study was supported by NCSU/NIH MBTP and by an NSF CAREER grant. We are grateful to Suk Tai Chang for his assistance with the FEMLAB modeling, to Nina Allen and Eva Johannes for the use of the Leica confocal microscope in the Cellular and Molecular Imaging Facility, and to Julian Willoughby for his assistance in performing the theta variation experiments.